JOURNAL OF GEOPHYSICAL RESEARCH, VOL. 109, E08005, doi:10.1029/2004JE002254, 2004

***Correction published 30 November 2004***

# Atmospheric rotational effects on Mars based on the NASA Ames general circulation model: Angular momentum approach

Braulio Sanchez, Robert Haberle, and James Schaeffer

Geodynamics Branch, Laboratory for Terrestrial Physics, NASA Goddard Space Flight Center, Greenbelt, Maryland, USA

Received 25 February 2004; revised 4 June 2004; accepted 16 June 2004; published 24 August 2004.

[1] The NASA Ames general circulation model has been used to compute time series for atmospheric products of inertia and relative angular momentum terms. Model outputs were used also to compute time series representing the inertia terms due to $CO_2$ condensation and sublimation on the surface of Mars. Some of these terms were used to generate time series representing the forcing functions for the equatorial components of the linearized Liouville equations of rotational motion. These equations were then solved numerically for a period of a Martian year (669 sols) to obtain a time series for the position of the rotation pole on the surface of Mars. The results of the investigation indicate that mass variation in the atmosphere is as important as the formation and sublimation of ice caps on the surface of the planet. Numerical integration of the equations of rotational motion yields pole displacements as large as 30.9 cm (ice caps solution), 39.5 cm (atmospheric effects), or 33 cm (both effects combined). Fourier analysis of the time series corresponding to the equatorial components of pole displacement for the ice caps solution as well as the atmospheric effects solution shows that the (1/3)-annual harmonic has the largest coefficient in three cases, with magnitudes in the 7–9 cm range. Fourier analysis of the equatorial components of polar motion for the combined solution yields main harmonics of 5.12 cm (x), (1/3)-annual and 7.50 cm (y), annual. *INDEX TERMS:* 0343 Atmospheric Composition and Structure: Planetary atmospheres (5405, 5407, 5409, 5704, 5705, 5707); 5450 Planetology: Solid Surface Planets: Orbital and rotational dynamics; 6225 Planetology: Solar System Objects: Mars; 6207 Planetology: Solar System Objects: Comparative planetology; *KEYWORDS:* atmospheric model, Mars, rotation

**Citation:** Sanchez, B., R. Haberle, and J. Schaeffer (2004), Atmospheric rotational effects on Mars based on the NASA Ames general circulation model: Angular momentum approach, *J. Geophys. Res.*, *109*, E08005, doi:10.1029/2004JE002254.

## 1. Introduction

[2] The rotational variations of a planet can be analyzed into axial and equatorial components. The axial variations (along the z axis, which is the rotation axis) are reflected in changes in the length of day (LOD). The equatorial variations (x, y) produce changes in the orientation of the axis of rotation (polar motion). The solution of Liouville's equations provides the changes in planetary rotation, i.e., changes in LOD and polar motion, as discussed by *Lambeck* [1980].

[3] The methodology of planetary rotational investigations can follow the angular momentum approach or the torque approach. The chosen methodology determines the boundaries of the appropriate control volume. The angular momentum method involves the computation of terms containing the products of inertia of the atmosphere ("mass terms") and their time derivatives, as well as relative angular momentum terms ("motion terms") and their derivatives.

[4] The objective of this investigation is to use the angular momentum methodology to compute and analyze how the atmosphere affects Mars' polar motion, based on outputs from the NASA Ames General Circulation Model (GCM). The model provides values of wind velocity, density and pressure, which serve as inputs to the calculation of the terms which appear in Liouville's equations of rotational motion.

[5] The torque approach was used in a previous investigation by *Sanchez et al.* [2003], referred below as Paper I, to compute polar motion and LOD variations. The LOD variations were computed also using the angular momentum methodology. Mars' solid body was modeled as rigid, with the Love number $k_2 = 0$. The polar motion effects produced by the ice caps products of inertia were not computed since the necessary data was not available then.

[6] The studies of atmospheric effects on the rotation of Mars constitute a growing body of scientific literature. Paper I provides a number of references. Many of these works were concerned only with seasonal variations in the rotation rate (LOD). Those which computed polar motion variations are discussed in a section below.

[7] The model used here for the body of Mars does not include a liquid core or a solid inner core; therefore associated near-diurnal and other possible resonances are excluded. We hope to study them in a future work. Mars'

solid body is considered as elastic with a value of the Love number $k_2 = 0.153$, as determined by *Yoder et al.* [2003] from analysis of Mars Global Surveyor radio tracking.

[8] The paper presents the results of Fourier analysis of time series representing various quantities. For each pair of terms, $a_k \cos kt + b_k \sin kt = (a_k^2 + b_k^2)^{1/2} \cos(kt\text{-}\varphi)$, we refer to the quantity $(a_k^2 + b_k^2)^{1/2}$ as the "power at frequency k". A plot of this quantity as a function of k is called the power spectrum, as shown by *Hamming* [1986, p. 515]. Note that this convention makes the units of power the same as those of the particular time series under consideration, i.e., if the time series refers to displacement in cm, then the units of power are cm also. When reference is made to "total power", it is meant the sum over the entire frequency range. Excitation or forcing function magnitudes are given in Hadley units. One Hadley (H) is equal to $10^{18}$ Newton-meters.

[9] The structure of the paper is as follows. The Liouville equations of rotational motion are introduced in section 2. Time series and analysis of the equatorial excitation functions are treated in section 3. The computation of polar motion constitutes the subject of section 4. Section 5 presents a comparison of the results using the torque approach and the angular momentum approach. A comparison of the results with previous investigations is the subject of section 6. Summary and conclusions appear in section 7.

## 2. Liouville Equations

[10] Liouville gave the basic equations of motion in 1858. A linearized form of the equatorial components is given by *Munk and MacDonald* [1975]:

$$\begin{aligned} A(\omega_x)' + (C - B)\Omega\,\omega_y &= -(h_x - \Omega\, I_{xz})' + \Omega(h_y - \Omega\, I_{yz}) + L_x \\ B(\omega_y)' - (C - A)\Omega\,\omega_x &= -(h_y - \Omega\, I_{yz})' - \Omega(h_x - \Omega\, I_{xz}) + L_y, \end{aligned} \tag{1}$$

where A and B are the equatorial moments of inertia, C is the polar moment of inertia, $I_{yz}$ and $I_{xz}$ are the products of inertia, $h_x$ and $h_y$ are the relative angular momentum terms. $\Omega$ is the mean angular speed of rotation, $\omega_x$ and $\omega_y$ are the equatorial components of angular velocity. $L_x$ and $L_y$ are the equatorial components of external torque. The primes denote derivatives with respect to time.

[11] The time-varying parts of the products of inertia can be separated into three components: (1) a part due to the rotational deformation of the solid body of the planet, (2) a part due to the $CO_2$ and $H_2O$ ices condensing and subliming on the surface of the planet, and (3) a part due to the mass redistribution of the atmosphere. The expressions for the products of inertia can then be written as follows:

$$\begin{aligned} I_{yz} &= -\left[k_2 R^5 \Omega/(3G)\right]\omega_y + \left(1 + k_2^1\right)\left[(\Delta I_{yz})_a + (\Delta I_{yz})_s\right] \\ I_{xz} &= -\left[k_2 R^5 \Omega/(3G)\right]\omega_x + \left(1 + k_2^1\right)\left[(\Delta I_{xz})_a + (\Delta I_{xz})_s\right]. \end{aligned} \tag{2}$$

[12] The first term in equation (2) is the rotational deformation part [*Munk and MacDonald*, 1975]. The second term denotes the atmospheric part. The contribution due to surface ice is indicated by the third term, $k_2$ is the second-degree tidal effective Love number, $k_2^1$ is the second-degree loading Love number, R is the radius of the planet, and G is the gravitational constant.

[13] Substituting equation (2) into equation (1) and solving for $\omega_x$ and $\omega_y$ yields

$$\mathbf{Y}' - \mathbf{N}\,\mathbf{Y} = \mathbf{F}_a + \mathbf{F}_s + \mathbf{L} \tag{3}$$

$$\mathbf{Y} = \left[c_1\,\omega_x, c_2\,\omega_y\right]^T \tag{4}$$

$$\mathbf{N} = \text{matrix} \begin{matrix} 0 & -d_1 \\ d_2 & 0 \end{matrix} \tag{5}$$

$$\mathbf{F}_a = \left[F_{ax}, F_{ay}\right]^T \tag{6}$$

$$\begin{aligned} F_{ax} &= \left(1 + k_2^1\right)\left[\Omega\,\Delta I'_{xz} - \Omega^2\,\Delta I_{yz}\right]_a + \Omega\, h_y - h'_x \\ F_{ay} &= \left(1 + k_2^1\right)\left[\Omega\,\Delta I'_{yz} + \Omega^2\,\Delta I_{xz}\right]_a - \Omega\, h_x - h'_y \end{aligned} \tag{7}$$

$$\mathbf{F}_s = \left[F_{sx}, F_{sy}\right]^T \tag{8}$$

$$\begin{aligned} F_{sx} &= \left(1 + k_2^1\right)\left[\Omega\,\Delta I'_{xz} - \Omega^2\,\Delta I_{yz}\right]_s \\ F_{sy} &= \left(1 + k_2^1\right)\left[\Omega\,\Delta I'_{yz} + \Omega^2\,\Delta I_{xz}\right]_s \end{aligned} \tag{9}$$

$$\mathbf{L} = \left[L_x, L_y\right]^T \tag{10}$$

$$c_1 = A + k_2 R^5 \Omega^2/(3G) \tag{11}$$

$$c_2 = B + k_2 R^5 \Omega^2/(3G) \tag{12}$$

$$d_1 = \Omega\left[(C - B) - k_2 R^5 \Omega^2/(3G)\right] \tag{13}$$

$$d_2 = \Omega\left[(C - A) - k_2 R^5 \Omega^2/(3G)\right], \tag{14}$$

where the superscript "T" denotes transposed.

[14] The solution of equation (3) provides the trajectory of the point of intersection of the axis of rotation with the surface of the planet by the well-known relations

$$\begin{aligned} x &= (\omega_x/\Omega)\,R \\ y &= (\omega_y/\Omega)\,R. \end{aligned} \tag{15}$$

[15] The value of the polar moment of inertia C used in the calculations was obtained from

$$C = 0.366\,M R^2, \tag{16}$$

**Table 1.** Chandler Period as a Function of Triaxiality and Elasticity[a]

| Moments of Inertia | $k_2$ | Chandler Period |
|---|---|---|
| A, A, C | 0. | 196.8 |
| A, B, C | 0. | 186.1 |
| A, A, C | 0.153 | 225.4 |
| A, B, C | 0.153 | 211.6 |

[a]A = 2.68594 ($10^{36}$) kg-m$^2$, B = 2.68433 ($10^{36}$) kg-m$^2$, C = 2.69956 ($10^{36}$) kg-m$^2$. Chandler period in sols.

where $M = 6.4185 \times 10^{23}$ kg and R = 3389920 m [*Sohl and Spohn*, 1997] and $\Omega = 0.7088 \times 10^{-4}$ sec$^{-1}$. The values of the equatorial moments of inertia A and B follow from the values of the gravitational coefficients $C_{20}$ and $C_{22}$ and the value of C:

$$A = M R^2 (C_{20} + 0.366 - 2.\, C_{22}) \tag{17}$$

$$B = M R^2 (C_{20} + 0.366 + 2.\, C_{22}). \tag{18}$$

The values for the gravitational coefficients are those given by *Lemoine et al.* [2001].

[16] By setting the forcing functions equal to zero in equation (3), the eigenvalues of matrix **N** yield the associated Martian Chandler period:

$$P = 2\pi / [(d_1\, d_2)/(c_1\, c_2)]^{1/2}. \tag{19}$$

[17] Letting A = 2.68594 ($10^{36}$) kg-m$^2$, B = 2.68433 ($10^{36}$) kg-m$^2$, C = 2.69956 ($10^{36}$) kg-m$^2$, and $k_2 = 0.153$ [*Yoder et al.*, 2003], the following values for the Martian Chandler period are obtained, as shown in Table 1.

[18] It is seen that triaxiality, with B < A, decreases the Chandler period by 10 days for a rigid Mars. For an elastic Mars, the reduction is 14 days. Elasticity increases the Chandler period: 29 days for a rotationally symmetric Mars, and 25 days for a triaxial Mars.

## 3. Excitation Functions

[19] General circulation models are widely used in the forecasting of weather and climate as well as in meteorological research. Given a set of initial conditions for temperature, pressure, wind fields, etc., the model uses the appropriate equations from fluid dynamics and radiative transfer theory to compute the evolution of the dynamical system by numerical integration both in time and space. The main energy source for the atmospheric motions is radiative transfer of solar energy, which is a function of Mars' orbital and rotational motions. Absorption, emission, and scattering of radiation by $CO_2$ and suspended dust is also included in the models.

[20] The NASA Ames GCM used here is one of the most sophisticated general circulation models for Mars. Very detailed descriptions can be found in the literature [e.g., *Pollack et al.*, 1990]. The description provided here is brief and not intended to exhaustively repeat material already covered in the available references.

[21] The NASA Ames GCM is a finite difference model based on the primitive equations of meteorology expressed in spherical sigma coordinates. The resolution is 7.5° (latitudinal) by 9° (longitudinal). The version of the model used here has 30 vertical layers extending from the surface to 100 km. The output files are written every 1.5 hours of simulated time, 16 times per sol. There are 10704 records in the data file, representing a time span of 669 sols (687 Earth days) which is the length of the Martian year.

[22] Kinetic energy is dissipated in the model by frictional interaction with the surface and a "sponge" layer at the model top. Surface friction is parameterized using an adaptation of the bulk boundary layer scheme of *Deardorff* [1972]. The sponge layer exists in the top three layers and is based on a simple Rayleigh friction scheme.

[23] The model allows for the condensation of $CO_2$ in the atmosphere as well as on the surface. The surface topography adopted in the model used in this investigation is based on a 1° × 1° MOLA topographic surface. An averaging and weighting procedure is used to create the final 7.5° × 9° data set.

[24] The outputs from the NASA Ames GCM provide a 1.5 hour sampling rate; therefore the results for the forcing functions are not limited to annual and semi-annual components.

[25] The condensation and sublimation of $CO_2$ on the surface and in the atmosphere of Mars produce changes in the atmospheric mass distribution as well as changes in the polar caps. From the standpoint or rotational dynamics these changes are manifested in time variations in the moments and products of inertia. Another source of rotational variations is due to the atmospheric winds, which contribute to the relative angular momentum terms.

[26] Figure 1 exhibits the time series for mass variation in the atmosphere and the ice caps. Note that they are negatives of each other, which indicates mass conservation is satisfied. The atmospheric variation occurs with respect to a mean value of 236 ($10^{14}$) kg, the ice mass variation has a mean of 35 ($10^{14}$) kg. Total power is 39 ($10^{14}$) kg for each series. The main harmonics are annual, semiannual, (1/3)-annual, and (1/4)-annual.

[27] The products of inertia variations appearing in equation (2) and the relative angular momentum terms are computed from the following expressions:

$$(\Delta I_{xz})_a = \int_V \rho_a\, r^2\, \sin\phi\, \cos\phi\, \cos\lambda\, dV \tag{20}$$

$$(\Delta I_{yz})_a = \int_V \rho_a\, r^2\, \sin\phi\, \cos\phi\, \sin\lambda\, dV \tag{21}$$

$$(\Delta I_{xz})_s = \int_V \rho_s\, r^2\, \sin\phi\, \cos\phi\, \cos\lambda\, dV \tag{22}$$

$$(\Delta I_{yz})_s = \int_V \rho_s\, r^2\, \sin\phi\, \cos\phi\, \sin\lambda\, dV \tag{23}$$

$$h_x = \int_V \rho_a\, r\, (v \sin\lambda - u\, \sin\phi\, \cos\lambda) dV \tag{24}$$

$$h_y = \int_V \rho_a\, r(-v\, \cos\lambda - u\, \sin\phi\, \sin\lambda) dV, \tag{25}$$

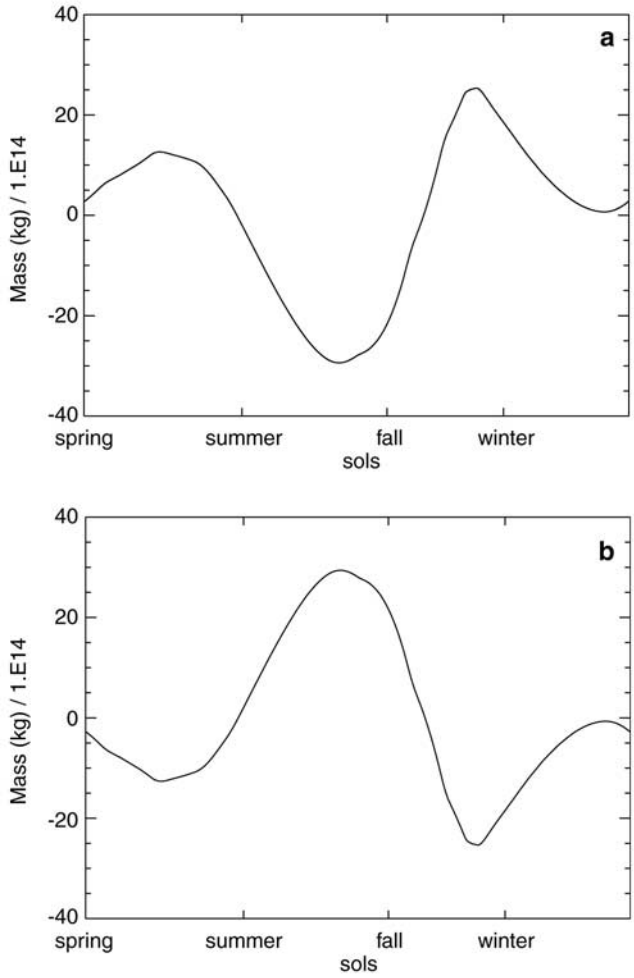


**Figure 1.** Mass variation time series. (a) Atmosphere. (b) Ice caps.

where $\rho_a$ is the atmospheric density, $\rho_s$ is the ice density, r is the distance from the center of planet, $\phi$ is latitude, $\lambda$ is east longitude, u is the eastward velocity component, v is the northward velocity component, and V stands for the volume of the atmosphere. The products of inertia variations appearing in equations (20)–(23) are computed from mass variations in the atmosphere or on the ice caps. The NASA/Ames GCM supplies inputs for both.

[28] The linearized Liouville equations, in the form of equation (3), show forcing functions on the right side due to atmospheric wind and mass changes and to ice formation and sublimation. If the angular momentum approach is taken, these forcing functions will drive the forced solution and no torque due to the atmosphere will appear in the control volume. Equations (7) and (9) give the atmospheric and ice contributions respectively.

[29] Some of the terms appearing in the forcing functions are associated with a redistribution of mass over the Earth' surface, the effects of loading and self-attraction have to be considered. This is done by means of the loading Love number $k_2^l$. The value of $k_2^l$ is weakly dependent on frequency [*Defraigne et al.*, 2000]; here an average value of $k_2^l = -0.06$ is adopted for the computations.

[30] Figures 2 and 3 present the time series and power spectra for the equatorial components of the atmospheric forcing functions. Figures 4 and 5 portray the results for the ice caps excitation functions. Tabulated results based on power spectrum analysis are given in Table 2. Note that the main harmonics for the ice caps excitation functions are all long periodic: annual, semiannual, (1/3)-annual, etc. The excitation functions based on atmospheric effects exhibit daily and sub-daily harmonics among the five most powerful. Figures 6 and 7 show time series and power spectra for the equatorial components corresponding to the sum of ice caps and atmospheric forcing. Tabulated results appear in Table 3. As expected, annual, semiannual, (1/3)-annual, daily and sub-daily harmonics rank among the most powerful.

[31] The forcing function frequencies appearing in Tables 2 and 3 do not have the same order in the power ranking. These differences must be the result of asymmetries in surface topography [*Van den Acker et al.*, 2002]. The complex interactions of the atmosphere with the topography can produce a rich spectrum of responses [*Read and Lewis*, 2004].

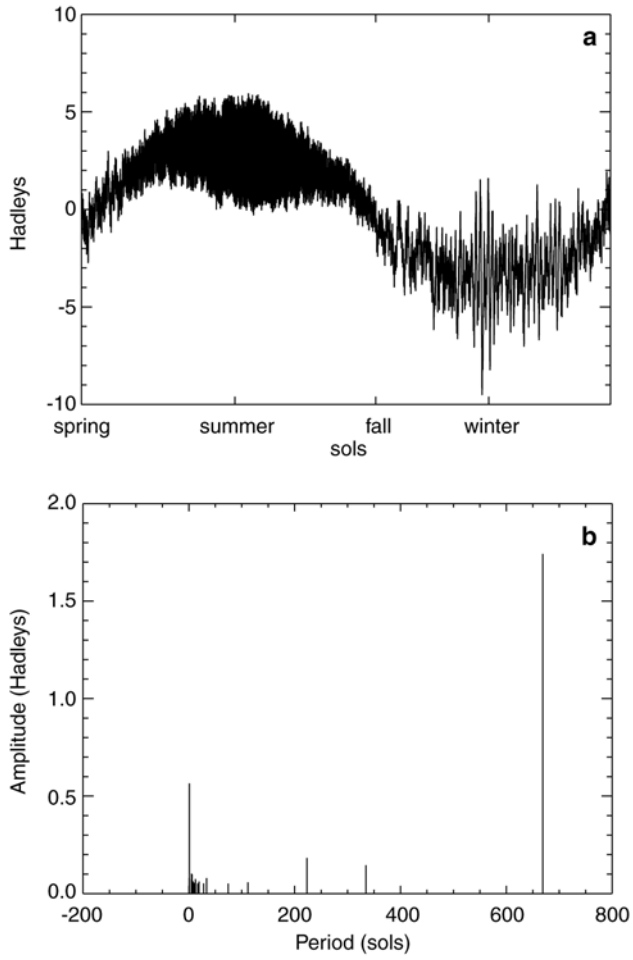


**Figure 2.** Atmospheric variation forcing function: X component. Amplitude in Hadleys. One Hadley is equal to $10^{18}$ Newton-meters. (a) Time series. (b) Power spectrum.

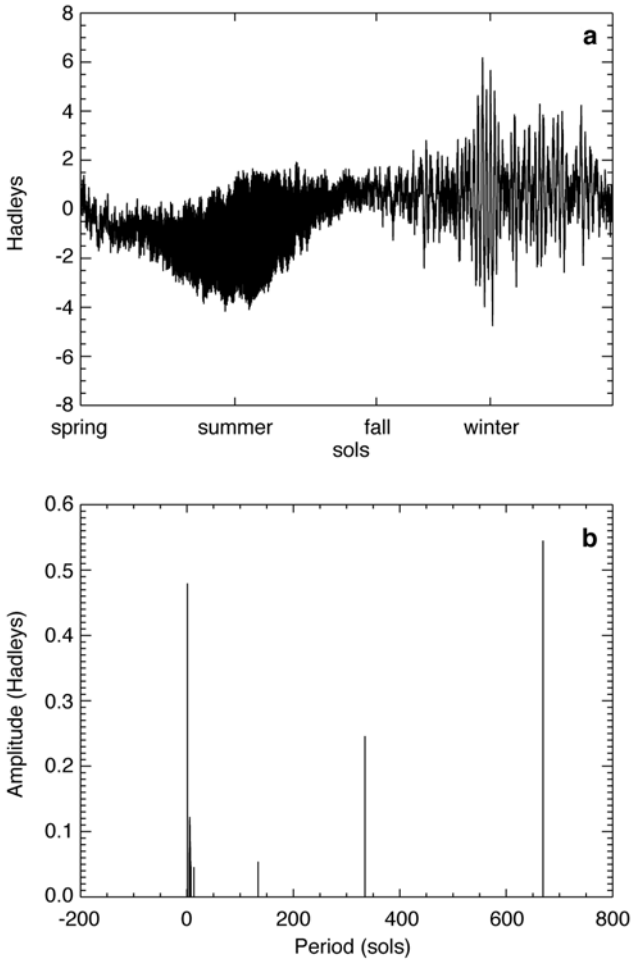


**Figure 3.** Atmospheric variation forcing function. Y component. (a) Time series. (b) Power spectrum.

[32] The long period harmonics are associated with seasonal effects, involving the revolution of Mars around the Sun and the inclination of its rotation axis with respect to the plane of the orbit. Mars' obliquity and the eccentricity of its orbit are greater than those of Earth, resulting in very pronounced seasons and large variations in the atmosphere, including the $CO_2$ condensation and sublimation cycle.

[33] Daily and sub-daily periods are associated with the daily rotational motion. Mars' strong daily cycle is due to the low thermal inertia of the atmosphere and the strong solar heating during the day [*Read and Lewis*, 2004], with day-night temperature differences reaching 100K. The surface also has a low thermal capacity due to the absence of oceans, cooling rapidly as night falls, as in desert landscapes on Earth.

[34] The magnitude = $(x^2 + y^2)^{1/2}$, of forcing due to ice caps condensation and sublimation reaches its maximum (2.22 H) at the end of the northern hemisphere summer (320 sols). This is approximately the time when total mass variations reach a maximum in the ice caps and in the atmosphere (313 sols). The forcing magnitude associated with atmospheric effects reaches its maximum (6.92 H) at the very end of the fall (505 sols), coincident with the maximum variation in atmospheric products of inertia: $\Delta I_{xz}$ (505 sols) and $\Delta I_{yz}$ (507 sols). The combined effect (ice plus atmosphere) reaches a maximum of 6.92 H at 505 sols.

## 4. Computation of Polar Motion

[35] The trajectory of the point of intersection of the rotation axis with the surface of Mars is obtained from equation (15), which requires the solution of equation (3).

[36] *Klein and Sommerfeld* [1914] have given the following general solution to equation (1) for the biaxial case (A = B):

$$\omega_x = g_1 \cos nt - g_2 \sin nt + (F\beta + G\beta') \cos ft - (F\eta - G\eta') \sin ft \quad (26)$$

$$\omega_y = g_2 \cos nt + g_1 \sin nt + (F\beta - G\beta') \sin ft + (F\eta + G\eta') \cos ft \quad (27)$$

$$F = (f + \Omega)/[A(f - n)] \quad (28)$$

$$G = (f - \Omega)/[A(f + n)], \quad (29)$$

where $g_1$, $g_2$, $\beta$, $\eta$, $\beta'$, and $\eta'$ are real constants, n is the natural or resonance (Chandler) frequency of the system,

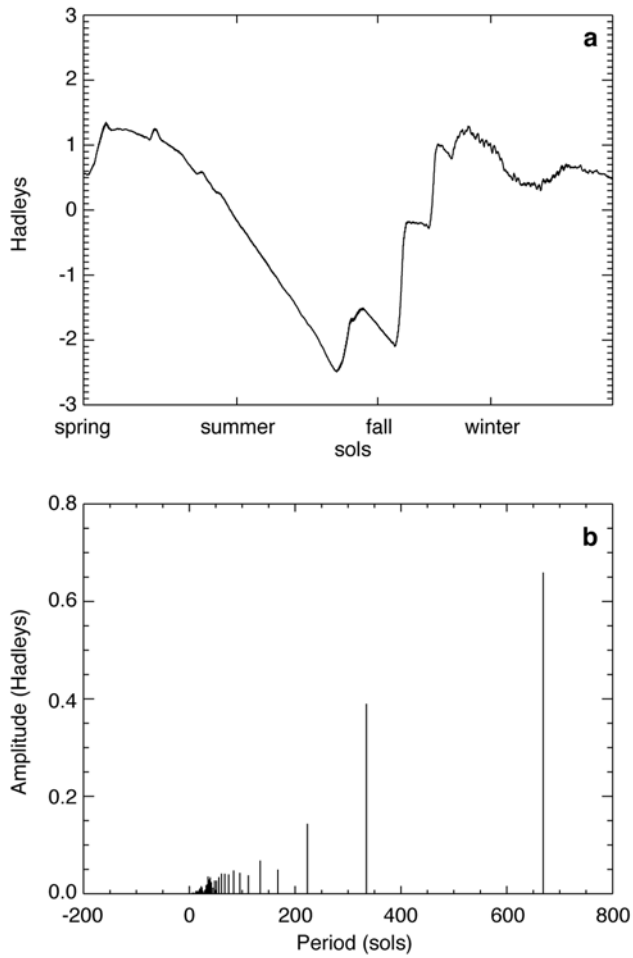


**Figure 4.** Ice caps variation forcing function: X component. (a) Time series. (b) Power spectrum.

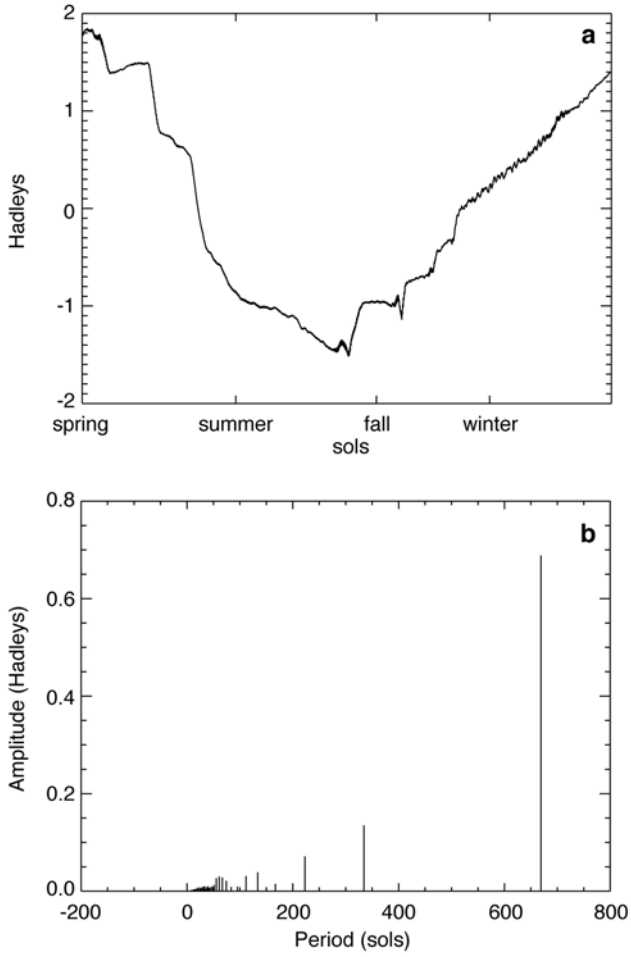


**Figure 5.** Ice caps variation forcing function: Y component. (a) Time series. (b) Power spectrum.

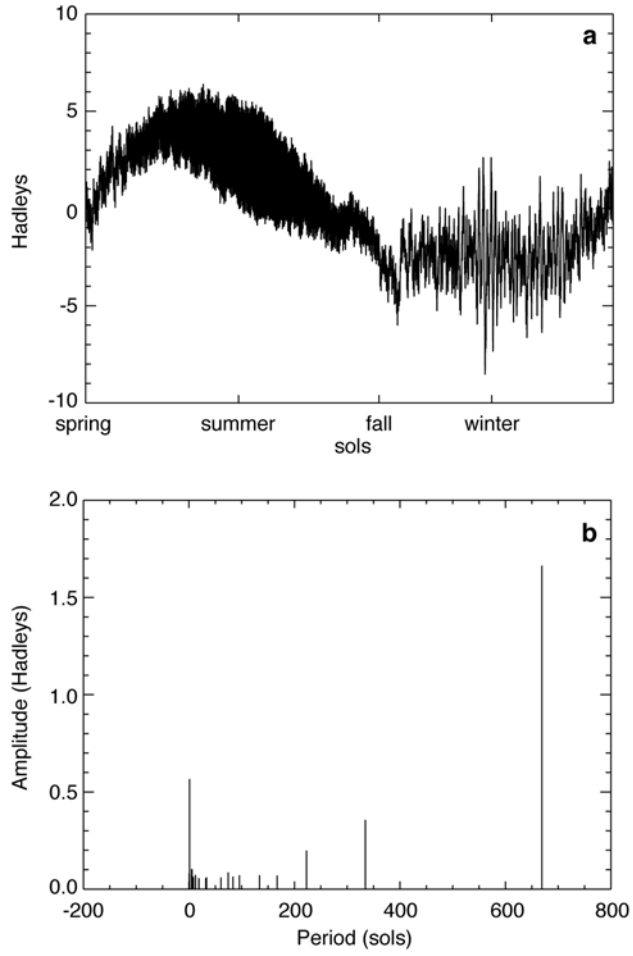


**Figure 6.** Atmospheric variation plus ice caps variation forcing function: X component. (a) Time series. (b) Power spectrum.

and f is the forcing frequency. As before, $\Omega$ is the mean angular speed of rotation. Note that if the forcing frequency is close to the Chandler frequency resonance might occur. Note also that if the forcing frequency is close to the mean angular speed, the magnitude of the forced response could decrease accordingly. A similar behavior can be expected for the triaxial case, when $A \neq B$.

[37] In this investigation the solution for the triaxial case is obtained by means of a numerical integration package using

**Table 2.** Main Harmonics of Forcing Functions and Equatorial Polar Motion Displacements Due to Ice Caps and Atmospheric Variations[a]

| Ice Caps Variations | | | | Atmospheric Variations | | | |
|---|---|---|---|---|---|---|---|
| Forcing Function | | Pole Displacement | | Forcing Function | | Pole Displacement | |
| Frequency | Amplitude | Frequency | Amplitude | Frequency | Amplitude | Frequency | Amplitude |
| | | | *X Component* | | | | |
| 1 | 0.66 | 3 | 8.99 | 1 | 1.74 | 3 | 7.88 |
| 2 | 0.39 | 1 | 4.09 | 669 | 0.56 | 1 | 4.28 |
| 3 | 0.14 | 2 | 2.15 | 668 | 0.20 | 2 | 3.90 |
| 5 | 0.07 | 4 | 2.00 | 670 | 0.19 | 4 | 2.55 |
| 4 | 0.05 | 5 | 1.56 | 3 | 0.18 | 5 | 0.95 |
| | | | *Y Component* | | | | |
| 1 | 0.69 | 3 | 8.51 | 1 | 0.54 | 1 | 9.40 |
| 2 | 0.14 | 2 | 4.06 | 669 | 0.48 | 3 | 6.81 |
| 3 | 0.07 | 1 | 2.99 | 2 | 0.25 | 4 | 2.78 |
| 5 | 0.04 | 4 | 1.53 | 671 | 0.16 | 2 | 2.24 |
| 6 | 0.03 | 5 | 1.06 | 667 | 0.15 | 5 | 1.26 |

[a]Frequency in cycles per year. Amplitudes of forcing functions in Hadleys. Amplitudes of polar motion displacements in cm.

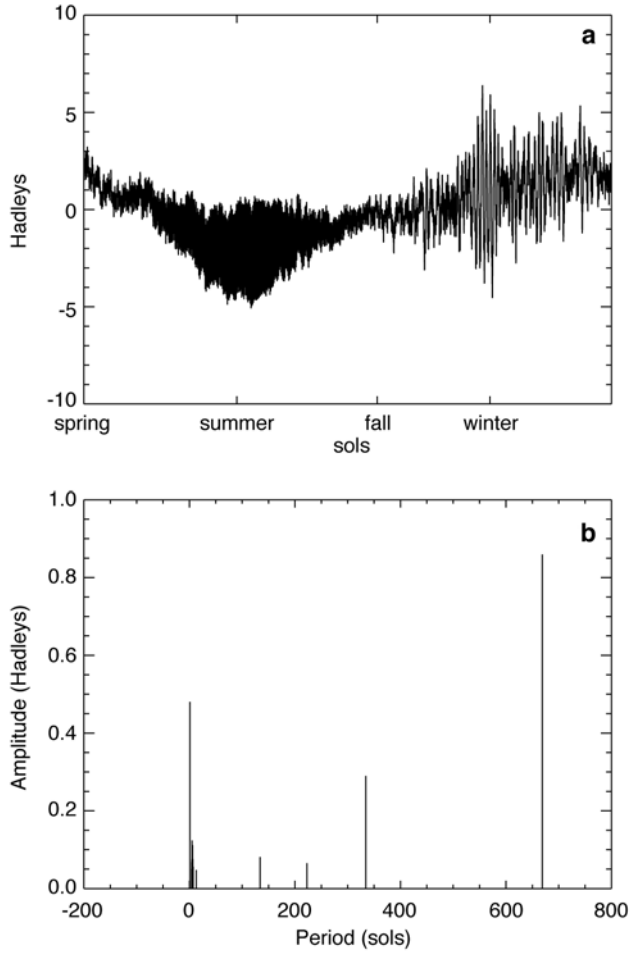


**Figure 7.** Atmospheric variation plus ice caps variation forcing function: Y component. (a) Time series. (b) Power spectrum.

the Runge-Kutta-Fehlberg (4,5) method with step size control [*Fehlberg*, 1969]. The solution thus obtained encompasses the response to all the frequencies present in the forcing function. Analysis of the resulting time series by fast Fourier transform methods yields the power content for each frequency. The main objective of the investigation is to determine and compare the effects due to variations in the atmosphere and in the ice caps. In addition, the dynamical system is linear, so that without loss of generality we can choose the initial conditions such that the pole of rotation is initially at the origin, $\omega_x = \omega_y = 0$. Furthermore the objective of the investigation does not extend to a comparison with real data, which is not presently available.

[38] Equation (3) was solved separately for effects due to ice condensation and sublimation on the surface of the planet and for effects due to mass redistribution in the atmosphere. The total effect is obtained by addition, due to the linearity of the equations.

[39] Table 2 presents Fourier analysis results for the time series corresponding to the equatorial components of pole displacement for the ice caps solution as well as the atmospheric effects solution. The (1/3)-annual harmonic has the largest coefficient in three cases, with magnitudes in the 7–9 cm range. The coefficients of the main harmonics are of similar magnitude for the ice caps and for the atmospheric effects.

[40] It is possible to consider the (x, y) components of the polar displacement as components of a vector characterized by magnitude = $(x^2 + y^2)^{1/2}$ and phase = arctan (y/x). Time series of magnitude and phase, as well as power spectrum results for the polar displacement due to atmospheric variations are shown in Figure 8. Corresponding results for ice condensation and sublimation appear in Figure 9. Results for the combination of both are given in Figure 10.

[41] The maximum displacement due to ice is 30.9 cm, occurring at 548 sols. Atmospheric effects yield a maximum of 39.5 cm at 478 sols. The combined effect has a maximum of 33 cm at 616 sols.

[42] The phase angle time series for the solution due to ice condensation and sublimation indicates a spiral motion performing three revolutions about the origin over a Martian year. The solution based on atmospheric mass variations and the combined solution both portray a spiral motion performing two revolutions during the Martian year.

[43] Table 3 lists the main harmonics for the x and y components of the combined solution. Compare with the main harmonics associated with the forcing functions, which appear in Table 3 also. Note the (1/3)-annual harmonic, which is magnified by the proximity of its period (223 sols) to the natural period of 211 sols. The daily and sub-daily harmonics appearing in the forcing functions are not very powerful in the pole displacement spectra.

[44] The solutions discussed thus far have used a loading Love number $k_2^l = -0.06$, solutions corresponding to the case $k_2^l = 0$ (no self-attraction and loading effects) have been obtained also. The latter case yields maximum displacements of 32.8 cm (ice caps variation solution), 40.9 cm (atmospheric variation solution) and 35.3 cm (combined solution). Self-attraction and loading decreases the polar motion displacement by 1.9 cm (ice caps solution), 1.4 cm (atmospheric variation solution), and 2.3 cm (combined solution).

## 5. Comparison of the Torque and Angular Momentum Results

[45] The atmospheric torques acting on the solid body of Mars were computed in the investigation presented in Paper

**Table 3.** Main Harmonics of the Excitation Function Due to Ice and Atmospheric Variations Combined and Associated Pole Displacement[a]

| Forcing Function | | Pole Displacement | |
|---|---|---|---|
| Frequency | Amplitude | Frequency | Amplitude |
| *X Component* | | | |
| 1 | 1.66 | 3 | 5.12 |
| 669 | 0.57 | 1 | 3.75 |
| 2 | 0.36 | 2 | 3.19 |
| 668 | 0.20 | 4 | 2.28 |
| 3 | 0.20 | 5 | 1.43 |
| *Y Component* | | | |
| 1 | 0.86 | 1 | 7.50 |
| 669 | 0.48 | 3 | 5.66 |
| 2 | 0.29 | 2 | 2.52 |
| 671 | 0.16 | 4 | 2.35 |
| 667 | 0.15 | 5 | 1.43 |

[a]Frequency in cycles per year. Forcing function amplitude in Hadleys. Pole displacement amplitude in cm.

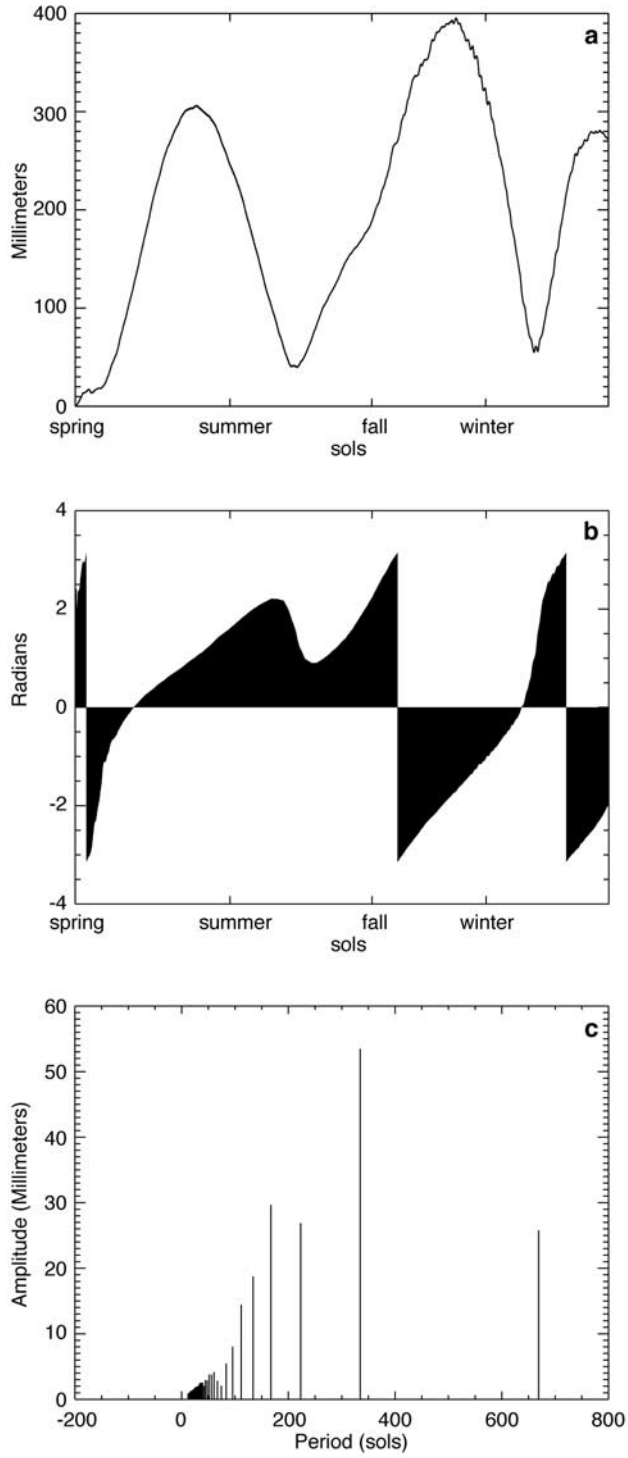


**Figure 8.** Polar motion due to atmospheric variations. (a) Displacement equals $(x^2 + y^2)^{1/2}$. (b) Phase equals arctan (y/x). (c) Power spectrum.

I. The associated polar motion was computed for a rigid Mars ($k_2 = 0$). However, in order to compute the total polar motion it is necessary to include ice condensation and sublimation effects on the surface of the planet. To compare with the results of this investigation the atmospheric torques computed in Paper I have been used as forcing functions on the right-hand side of equation (3). To match the conditions of this investigation Mars' solid body was considered elastic with a value of $k_2$ equal to 0.153. The results are presented in Figure 11. The solution due to ice condensation and sublimation has been presented above (Figure 9). The combined solution including atmospheric torques and

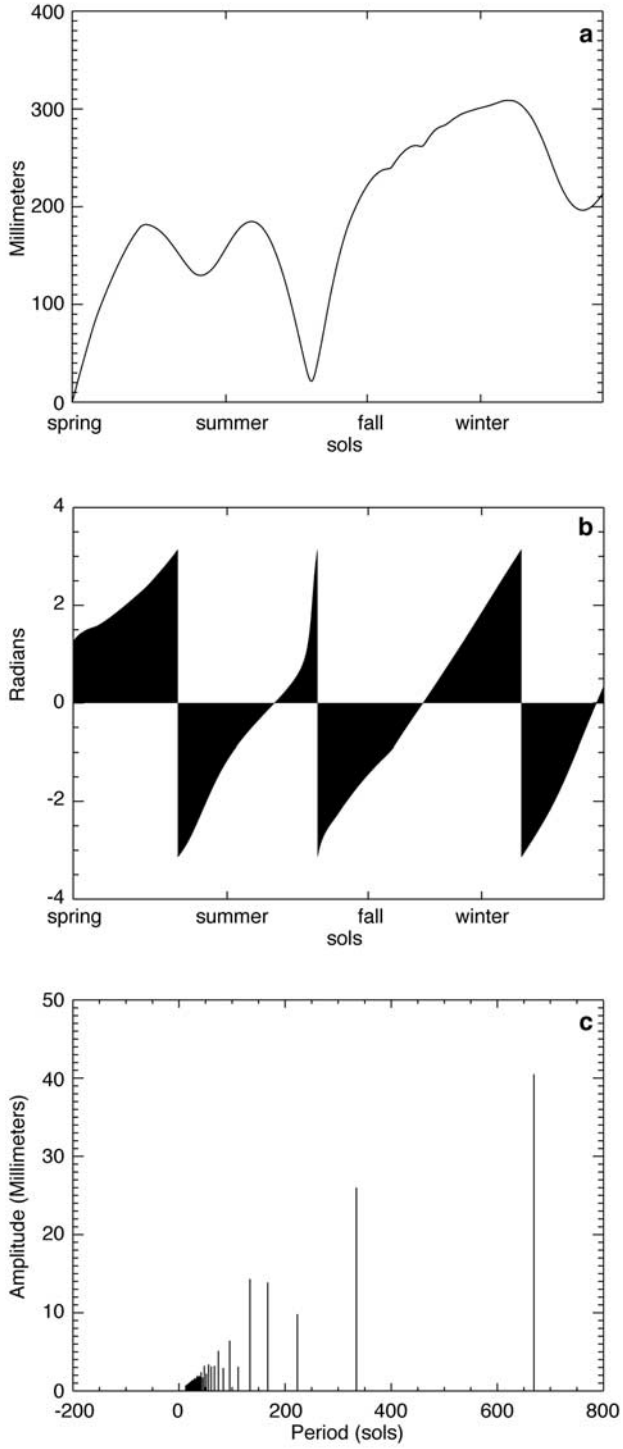


**Figure 9.** Polar motion due to ice caps variation. (a) Displacement equals $(x^2 + y^2)^{1/2}$. (b) Phase equals arctan (y/x). (c) Power spectrum.

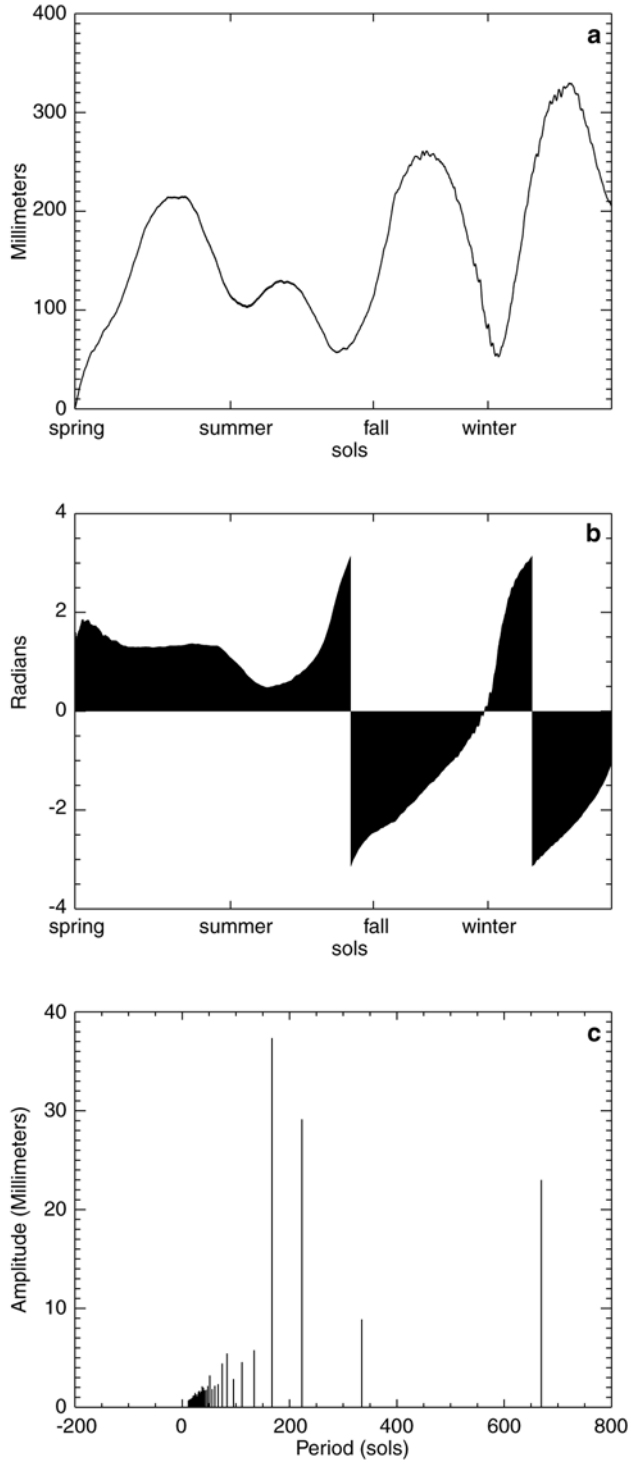


**Figure 10.** Polar motion due to atmospheric and ice caps variations combined. (a) Displacement equals $(x^2 + y^2)^{1/2}$. (b) Phase equals arctan (y/x). (c) Power spectrum.

ice caps effects is very similar to the one due to ice caps alone. The maximum displacement is 32 cm, occurring at 551.5 sols.

[46] The difference between the atmospheric variation/ice caps solution and the torque/ice caps solution is then equal to the difference between the atmospheric variation solution (Figure 8), and the torque solution (Figure 11). Figure 12a presents the time series corresponding to the magnitude of the difference. Figure 12b shows the power spectrum associated with the time series. It is clear that the atmospheric torques are not sufficiently powerful to match the polar motion solution generated by atmospheric variations.

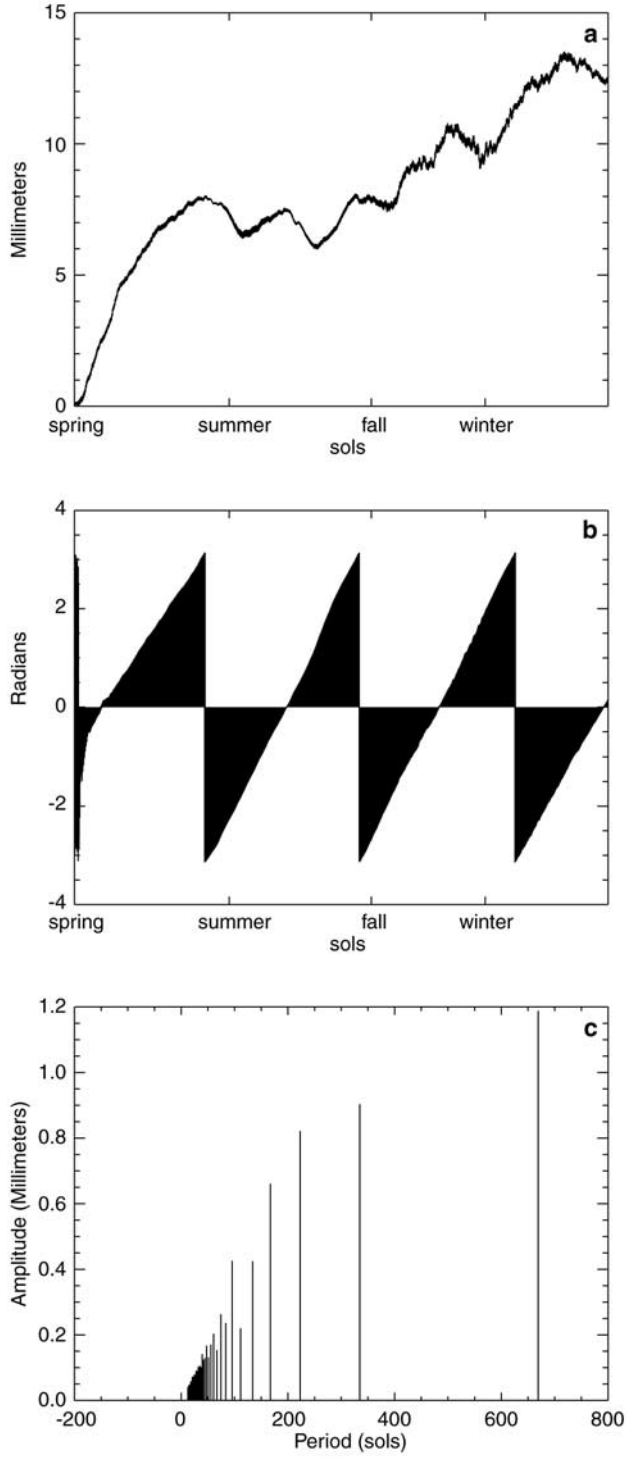


**Figure 11.** Polar motion due to atmospheric torques. (a) Displacement equals $(x^2 + y^2)^{1/2}$. (b) Phase equals arctan (y/x). (c) Power spectrum.

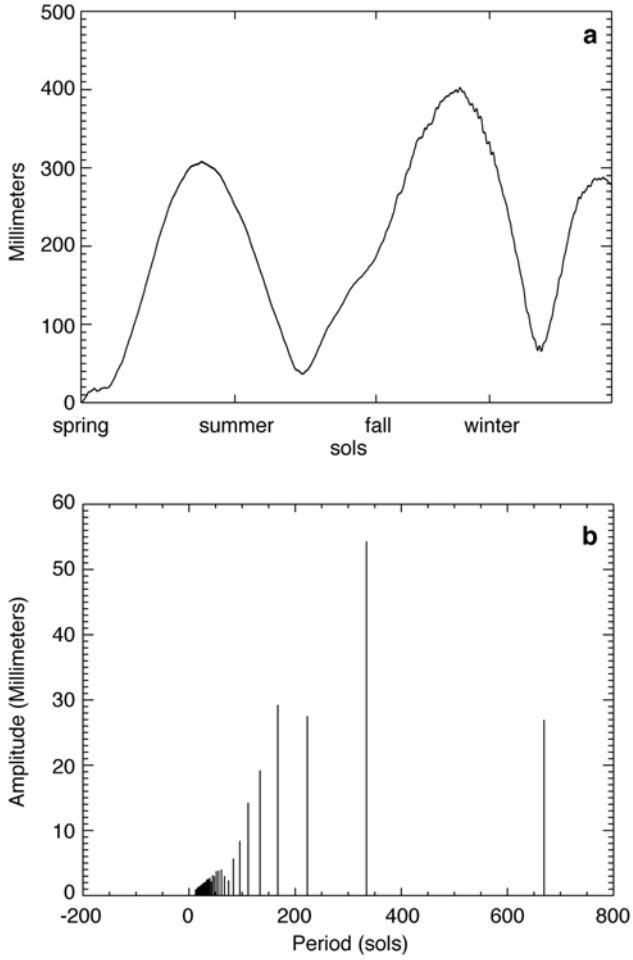


**Figure 12.** Difference between polar motion due to atmospheric variations (a.v.) and polar motion due to atmospheric torques (t.). (a) $[(x^2 + y^2)^{1/2}]_{a.v.} - [(x^2 + y^2)^{1/2}]_t$. (b) Power spectrum.

In theory the results from the torque approach and the results from the angular momentum approach should be identical. It is possible that the spatial grids used in the models are not sufficiently fine to achieve the necessary numerical accuracy conducive to a convergence of results for the two methodologies.

## 6. Comparison of Results With Other Investigations

[47] Polar motion results by other investigators are presented in Table 4. Due to differences in methodology, uncertainties in procedures used, lack of available details in the literature, etc. the comparison should be approached with caution. An effort has been made to make the comparison accurate. When in doubt, no entry was made in the table. Most of the previous investigations were concerned with the annual and semiannual harmonics only.

[48] The magnitudes presented in Table 4 for this investigation are obtained by taking the square root of the sum of the squares of the coefficients for the x and y components of polar motion appearing in Tables 2 and 3.

[49] *Chao and Rubincam* [1990] estimated that a 1° ice cap offset from the rotation axis would excite polar motion with an amplitude of 32 cm at the surface. The atmospheric effect was estimated at 20.8 cm.

[50] *Yoder and Standish* [1997] estimated the orientation of the Martian pole of rotation and axial rotation parameters for January 1, 1980 (midpoint in the Viking epoch). They used a model for the seasonal mass exchange between the ice caps and atmosphere to obtain estimates of polar motion due to asymmetric ice cap changes. These variations range from 16 to 32 cm at 1, 1/2, and 1/3 year, and 8 cm or less for 1/4 year. The relation between amplitude and period is associated with resonance effects caused by a wobble period estimated in the 193–212 day range.

[51] *Defraigne et al.* [2000] computed Mars' rotational variations using the output of a global circulation model for the Martian atmosphere developed by *Forget et al.* [1999]. Their polar motion results are 17.3 cm (annual) and 5.2 cm (semi-annual).

[52] *Van den Acker et al.* [2002] obtained total amplitudes of 12 cm on the surface for the annual and 9.7 cm for the semiannual polar motion excited by the atmosphere and ice caps. They used a version of the Mars GCM by *Forget et al.* [1999].

[53] The differences in polar motion magnitudes as obtained by the different investigations appear to be within reasonable limits, considering the probable differences in atmospheric models used.

## 7. Summary and Conclusions

[54] The NASA Ames general circulation model has been used to compute time series for atmospheric products of inertia and relative angular momentum terms. Model outputs were used also to compute time series representing the inertia terms due to $CO_2$ condensation and sublimation on the surface of Mars. Some of these terms were used to generate time series representing the forcing functions for the equatorial components of the linearized Liouville equations of rotational motion. These equations were then solved numerically to obtain a time series for the position of the rotation pole on the surface of Mars.

**Table 4.** Polar Motion Results From Various Investigations[a]

| | Polar Motion, cycles per year | | |
|---|---|---|---|
| Investigation | Ice Caps | Atmosphere | Ice Caps and Atmosphere Combined |
| *Chao and Rubincam* [1990] | 32 (1, 1/2)[b] | 20.8 (1, 1/2) | |
| *Yoder and Standish* [1997] | 16–32 (1, 1/2, 1/3)<br>8 (1/4) | | |
| *Defraigne et al.* [2000] | | | 17.3 (1)<br>5.2 (1/2) |
| *Van den Acker et al.* [2002] | 6.1 (1)<br>4.4 (1/2) | | 12.0 (1)<br>9.7 (1/2) |
| This investigation | 5.1 (1)<br>4.6 (1/2)<br>12.4 (1/3)<br>2.5 (1/4)<br>1.9 (1/5) | 10.3 (1)<br>4.5 (1/2)<br>10.4 (1/3)<br>3.8 (1/4)<br>1.6 (1/5) | 8.4 (1)<br>4.1 (1/2)<br>7.6 (1/3)<br>3.3 (1/4)<br>2.0 (1/5) |

[a]Polar motion in cm.
[b]Assumes a 1° ice cap offset.

[55] The annual, semiannual and (1/3)-annual harmonics appear among the five most powerful in the equatorial power spectra for both the ice caps and atmospheric effects, daily and sub-daily harmonics are also prominent in the atmospheric forcing but not in the ice caps forcing.

[56] The results of the investigation indicate that mass variation in the atmosphere is as important as the formation and sublimation of ice caps on the surface of the planet. Numerical integration of the equations of rotational motion yields pole displacements as large as 30.9 cm (ice caps solution), 39.5 cm (atmospheric effects), or 33 cm (both effects combined). Fourier analysis of the equatorial components of polar motion for the combined solution yields main harmonics of 5.12 cm (x), (1/3)-annual and 7.50 cm (y), annual.

[57] The effects of self-attraction and loading were determined to be of the order of 2–3 cm for a value of the loading Love number $k_2^l = -0.06$.

[58] The Mars' model used in the investigation corresponds to a triaxial, elastic solid body without a fluid core. For the adopted parameter values, the associated natural or Chandler period is 211.6 sols. When forced by ice caps and atmospheric variations the response of the model is a function of the separation between the forcing frequency and the natural frequency (as shown by equations (26)–(29)). Consequently, the response to the (1/3)-annual harmonic of the forcing is magnified in the spectra corresponding to the equatorial components of polar motion. The response to the daily and quasi-daily harmonics of forcing is decreased in magnitude, as shown by equations (26)–(29) also. However, if an ellipsoidal fluid core were incorporated in the Mars' model, a near-diurnal natural frequency would appear which might magnify the response to the daily and sub-daily harmonics present in the forcing functions. Additional resonances might appear if a solid inner core is introduced in the model [*Dehant et al.*, 2003], including a quasi-diurnal free inner core nutation and an inner core wobble with a period longer than the Chandler wobble.

[59] The torque approach was used as well to compute polar motion. The polar motion displacements thus obtained were not congruent with the polar motion displacements obtained using the angular momentum approach. Discrepancies between the two approaches have previously appeared in investigations concerned with atmospheric effects on the rotation of the Earth and Mars. Some authors have expressed their preference for the angular momentum approach [e.g., *Defraigne et al.*, 2000]. At the present time the quantity and quality of Mars' rotational data is not sufficient to ascertain which methodology is producing more realistic results. However, the amplitudes of the main harmonics as obtained in this investigation are certainly within the range of detection of future geodetic missions to Mars, such as the planned and postponed NetLander Ionospheric and Geodesic Experiment (NEIGE).

[60] Future investigations will benefit from the refinement of the atmospheric models to be expected as more and better data becomes available, as well as from more realistic models of Mars' inner structure.

[61] **Acknowledgments.** We are grateful to David P. Rubincam and an anonymous reviewer for their reading of the paper and their constructive remarks. We are grateful to Herbert V. Frey for providing encouragement and support as head of the Geodynamics Branch.

## References

Chao, B. F., and D. P. Rubincam (1990), Variations of Mars gravitational field and rotation due to seasonal $CO_2$ exchange, *J. Geophys. Res.*, *95*(B9), 14,755–14,760.

Deardorff, J. W. (1972), Parameterization of the planetary boundary layer for use in general circulation models, *Mon. Weather Rev.*, *100*, 93–106.

Defraigne, P., O. de Viron, V. Dehant, T. Van Hoolst, and F. Hourdin (2000), Mars rotation variations induced by atmosphere and ice caps, *J. Geophys. Res.*, *105*(E10), 24,563–24,570.

Dehant, V., T. Van Hoolst, O. de Viron, M. Greff-Lefftz, H. Legros, and P. Defraigne (2003), Can a solid inner core of Mars be detected from observations of polar motion and nutation of Mars?, *J. Geophys. Res.*, *108*(E12), 5127, doi:10.1029/2003JE002140.

Fehlberg, E. (1969), Low-order classical Runge-Kutta formulas with step-size control and their application to some heat transfer problems, *NASA Tech. Rep., NASA-TR-R-315*, 1 July.

Forget, F., F. Hourdin, R. Fournier, C. Hourdin, O. Talagrand, M. Collins, S. R. Lewis, P. L. Read, and J. P. Huot (1999), Improved general circulation models of the Martian atmosphere from the surface to above 80 km, *J. Geophys. Res.*, *104*(E10), 24,155–24,175.

Hamming, R. W. (1986), *Numerical Methods for Scientists and Engineers*, 2nd ed., Dover, Mineola, N. Y.

Klein, F., and A. Sommerfeld (1914), *Über die Theorie des Kreisels*, vol. I–III, Druck und Verlag, Liepzig.

Lambeck, K. (1980), *The Earth's Variable Rotation: Geophysical Causes and Consequences*, Cambridge Univ. Press, New York.

Lemoine, F. G., D. E. Smith, D. D. Rowlands, M. T. Zuber, G. A. Neumann, D. S. Chinn, and D. E. Pavlis (2001), An improved solution of the gravity field of Mars (GMM-2b) from Mars Global Surveyor, *J. Geophys. Res.*, *106*(E10), 23,359–23,376.

Munk, W. H., and G. J. F. MacDonald (1975), *The Rotation of the Earth*, Cambridge Univ. Press, New York.

Pollack, J. B., R. M. Haberle, J. Schaeffer, and H. Lee (1990), Simulations of the general circulation of the Martian atmosphere: 1. Polar processes, *J. Geophys. Res.*, *95*, 1447–1474.

Read, P. L., and S. R. Lewis (2004), *The Martian Climate Revisited*, Springer-Verlag, New York.

Sanchez, B. V., D. D. Rowlands, R. M. Haberle, and J. Schaeffer (2003), Atmospheric rotational effects on Mars based on the NASA Ames general circulation model, *J. Geophys. Res.*, *108*(E5), 5040, doi:10.1029/2002JE001984.

Sohl, F., and T. Spohn (1997), The interior structure of Mars: Implications from SNC meteorites, *J. Geophys. Res.*, *102*(E1), 1613–1635.

Van den Acker, E., T. Van Hoolst, O. de Viron, P. Defraigne, F. Forget, F. Hourdin, and V. Dehant (2002), Influence of the seasonal winds and the $CO_2$ mass exchange between atmosphere and polar caps on Mars' rotation, *J. Geophys. Res.*, *107*(E7), 5055, doi:10.1029/2000JE001539.

Yoder, C. F., and E. M. Standish (1997), Martian precession and rotation from Viking lander range data, *J. Geophys. Res.*, *102*(E2), 4065–4080.

Yoder, C. F., A. S. Konopliv, D. N. Yuan, E. M. Standish, and W. M. Folkner (2003), Fluid core size of Mars from detection of the solar tide, *Science*, *300*, 299–303.

R. Haberle, B. Sanchez, and J. Schaeffer, Geodynamics Branch, Laboratory for Terrestrial Physics, NASA Goddard Space Flight Center, Code 921, Greenbelt, MD 20771, USA. (braulio.v.sanchez@nasa.gov)